Acta Mech. Sin. (2011) 27(2):152–163
DOI 10.1007/s10409-011-0431-2

RESEARCH PAPER

Aerodynamics of indirect thrust measurement by the impulse method

Cheng-Kang Wu · Hai-Xing Wang · Xian Meng · Xi Chen · Wen-Xia Pan

Received: 14 December 2009 / Revised: 9 June 2010 / Accepted: 24 June 2010

Abstract The aerodynamic aspects of indirect thrust measurement by the impulse method have been studied both experimentally and numerically. The underlying basic aerodynamic principle is outlined, the phenomena in subsonic, supersonic and arc-heated jets are explored, and factors affecting the accuracy of the method are studied and discussed. Results show that the impulse method is reliable for indirect thrust measurement if certain basic requirements are met, and a simple guideline for its proper application is given.

Keywords Thrust measurement · Impulse method · Aerodynamic features · Cold jet · Arc-heated jet

1 Introduction

The force (thrust) exerted by a gas or liquid jet on the body (thruster) producing the jet is usually measured by directly mounting the thruster on a thrust stand and taking the measurement with a force measuring system, designed specifically for the range of force to be measured, from very large to the order of micro-Newtons. However, these direct methods are often not very practical. For instance, for complex experimental installations which are too large or heavy to be mounted as one item on the thrust stand, for mini- or micro-thrusters where the thrust is extremely small and any connecting tubes or wires might cause large errors, or in cases where the use of inexpensive and easy-to-operate devices is preferred over the elaborate and expensive thrust stands, other ways need to be employed. Indirect methods of measuring thrust have been used, mostly by measuring the impulse of the jet [1–7], or by using pitot tubes [8]. In many recent cases, the impulse method has been applied to mini- or micro-thrusters [5, 9, 10] for its convenience and relative simplicity. Most use a flat plate of large area as the element receiving the total impulse, but in cases where the flow is highly rarefied and reflections from the plate must be avoided, elaborate shapes other than the flat plate are used as the impulse receiver [5]. In an ion engine with charged particle stream, besides the flat plate for capturing momentum of the particles, a Faraday probe has been used to measure the ion flux, and a scan over the stream cross section is used to obtain the total impulse [2]. A large and heavy plate has been used to measure impulse in a larger installation [1]. The flat plate has also been used on combustion-powered test setups such as a pulse jet with ejectors, working in atmospheric environment [7]. The force of jets impinging on flat plates is also of interest in other problems such as blast from launch tubes [11]. The principle of indirectly measuring the jet thrust by impulse measurement is applicable to all kinds of gas or liquid jets working on the reaction principle. However, rarely has the aerodynamic aspects of the principle

The project was supported by the National Natural Science Foundation of China (50836007, 10921062, 10772016).

C.-K. Wu (✉) · X. Meng · W.-X. Pan
Institute of Mechanics, Chinese Academy of Sciences,
100190 Beijing, China
e-mail: ckw@imech.ac.cn

H.-X. Wang
School of Astronautics, Beijing University of Aeronautics and Astronautics, 100191 Beijing, China

X. Chen
Department of Engineering Mechanics,
Tsinghua University, 100084 Beijing, China

involved in these applications been studied. For instance, in Ref. [4], the force on a flat plate was measured as a function of distance from the nozzle exit, both in atmospheric and vacuum environments, but the resulting data still need to be better analyzed from an aerodynamic standpoint. When such a method is used indiscriminately under all conditions without knowing its condition of applicability and its range of validity, there is danger of unaccountable errors coming into the results of measurement. The purpose of this study is to better understand the phenomenon of impinging force exerted by a jet on a flat plate placed normally to the jet axis under various operating conditions and its relationship with the thrust force produced by the jet on the thruster, using the tools of aerodynamics. This would help to more clearly describe the validity, accuracy and limits of applicability of the indirect thrust measurement by the impulse method using a flat plate.

The study has been carried out experimentally and numerically, under atmospheric and low-pressure environmental conditions. In the experiments, cold nitrogen was used in most cases, but some data with arc-heated argon or N_2/H_2 as working gas have also been obtained. Force measurements and impact pressure measurements in the flow field were performed. In the numerical study, detailed aerodynamic equations for the studied case based on the momentum theorem were derived, and numerical computations for the cases of cold flow (where the continuum assumption generally holds) using the FLUENT software were performed to give a general idea of the picture of the flow field and trends of impact force variation under different conditions. It is noteworthy that the aim of these computations is mainly to help to understand the basic phenomena in the flow field and the general features of the indirect method of thrust measurement. Accurate comparison of the numerical and experimental results is not a main purpose, because of the complicated flow field and the relative crudeness of the methods. Possible effects of gas rarefaction in the case of arc-heated jet under low-pressure environment are briefly discussed. From these studies, better understanding of the phenomenon under various conditions is obtained, and a simple guideline for properly using the indirect method is given.

2 Basic idea for the impulse method of indirect thrust measurement

In an idealized and simplified version, the basic principle involved can be explained by applying the momentum theorem to the control volumes shown in Fig. 1.

(1) For a thruster (shown in Fig. 1a as a simple rocket) mounted on a test stand and working in the steady state, the momentum theorem for axial z-direction gives $T + (p_0 - p_e)A_e = z\text{-Momentum flux out} = \int v_z \mathrm{d}\dot{m}$, or $T = \int v_z \mathrm{d}\dot{m} - (p_0 - p_e)A_e$, where T is the force exerted by the test stand on the thruster, which is numerically equal to the thrust produced by the thruster in the given environment; p_0 is the environmental pressure; p_e and A_e are the gas pressure and section area at nozzle exit; $\mathrm{d}\dot{m}$ and v_z are the differential mass flux and related axial component of the exit velocity, respectively; whereas the integral covers the whole nozzle exit section.

(2) The boundary of the control volume, shown in Fig. 1b, includes both the thruster and the back side of the flat plate and is far enough so that the pressure on the boundary is equal to the environmental pressure p_0. The other forces acting on the boundary are the force T' exerted by the test stand on the thruster, and the force F exerted by the force transducer on the flat plate. In the case where the gas enters and leaves the control volume only in the radial direction, the momentum theorem for the z-direction gives $T' = F$, i.e., the force measured by the force transducer behind the flat plate is equal to the thrust measured by the thrust stand. The forces T and T' are not necessarily the same when there is an influence on the nozzle flow due to the presence of the flat plate. Therefore, the requirements for the measured force F equaled to the thrust force T are no axial momentum in or out of the control volume and no influence on nozzle flow by the presence of the plate. These are basic ideas behind the indirect measurement of thrust by the impulse method.

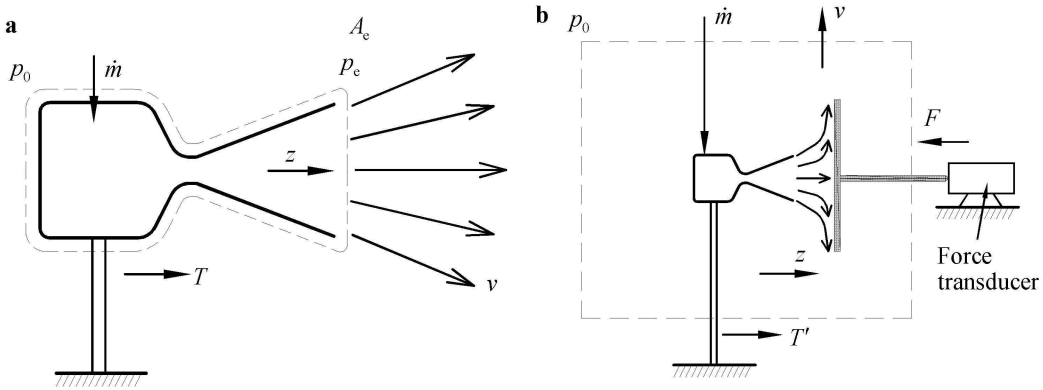

Fig. 1 Schematic diagram of the impulse method of indirect thrust measurement

However, these requirements are not automatically satisfied in all cases, for instance, in rarefied flow where the particles bounce off the plate in many directions, in cases where axial momentum is spilled over the edge of the plate, in charged particle flows where there might be other mechanisms affecting momentum transfer, or where the interaction between the plate and the flow might cause errors in inferring the test results. Therefore, a study in the aerodynamic aspects of these cases would be helpful in clarifying the flow situation and finding limitations to the validity or accuracy of the method.

The above discussion is valid for all kinds of jets, both subsonic and supersonic, so the application is quite general. A detailed derivation for equations to be used in numerical computation will be given in the later section.

2.1 Experimental

Experiments were carried out in the test chamber for electric thrusters at the Center for Plasma and Combustion Research (CPCR) of the Institute of Mechanics, Chinese Academy of Sciences (IMCAS). It is a stainless steel chamber with a diameter of 2 m and a length of 4 m, equipped with vacuum pumps, gas and power supplies, the test stand and traversing mechanisms, as well as a large number of diagnostic instrumentation systems. A schematic of experimental setup is shown in Fig. 2. Tests with cold nitrogen gas were conducted at both atmospheric pressure and low pressure environments, and hot plasma jets from a 1 kW-class arcjet thruster were tested under the low pressure condition. The nozzles producing the jets have a throat diameter of 0.8 mm and the conical expansion portion has a half-angle of 15° or 10°, with lengths of 11 mm, 18 mm, 12 mm, 6 mm, and 3.5 mm. The flat plate for thrust measurement has a diameter of 200 mm. Impact pressure measurements were performed with a pitot-type pressure probe and a pressure tap centrally positioned on a flat plate with a diameter of 280 mm, with a 0.9 mm hole in the probe tip and the plate center connected to a sensitive pressure transducer of the piezo-resistive type. The nozzles or the arcjets are mounted on tables movable by traversing mechanisms, which are in turn driven by two stepping-motors, providing axial or radial movement of the jet nozzle with respect to the fixed position of the measuring instruments. Because the instrumentations are of the fast-response type, data were taken during traverse of the measuring devices at speeds of several millimeters per second so that the readings can be considered quasi-stationary. Signals were recorded digitally on a computer.

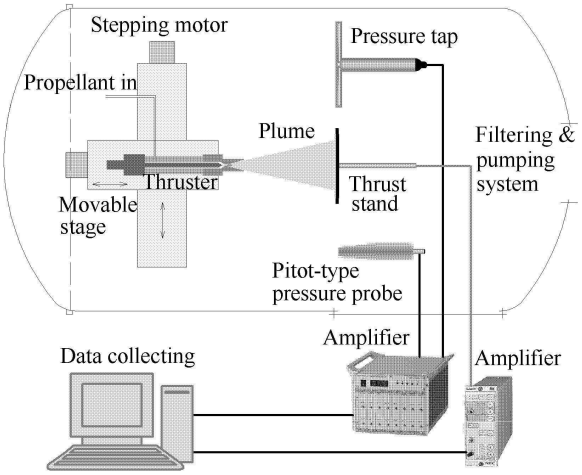

Fig. 2 Schematic diagram of the experimental system

2.2 Computational study

For the actual case that a viscous gas jet is exhausting from a thruster and impinging on a flat plate normal to the jet, ambient gas will be entrained into the gas jet. Viscous stresses and/or additional momentum flux will appear at the interfaces of the control volume, thus the relationship between the thrust force T and the force exerted on the plate F needs to be clarified. With fluid flowing through a control volume, the momentum theorem states [12,13]

$$\sum_i \boldsymbol{F}_i = \frac{\partial}{\partial t}\Big(\iiint_{\mathrm{cv}} \rho \boldsymbol{v} \mathrm{d}V\Big) + \iint_{\mathrm{cs}} \rho \boldsymbol{v}(\boldsymbol{v}\cdot\hat{\boldsymbol{n}})\mathrm{d}A, \tag{1}$$

where $\boldsymbol{F}_i$ is the i-th force vector, ρ is the gas density, $\boldsymbol{v}$ is the velocity vector, $\hat{\boldsymbol{n}}$ is the outward unit vector normal to the control surface, and cv and cs denote the integration over the control volume and the control surface, respectively. LHS is the vector sum of all forces acting on the system. The first term on the RHS is the change in total momentum vector due to unsteadiness, while the second term is the sum of convective momentum flux across the control surface (positive for outward momentum flux).

For steady flow and negligible body force, the momentum equation in the axial direction is written as

$$\sum_i F_{i,z} = \iint_{\mathrm{cs}} \rho v_z(\boldsymbol{v}\cdot\hat{\boldsymbol{n}})\mathrm{d}A, \tag{2}$$

where $F_{i,z}$ is the axial component of the force acting on the i-th surface, v_z is the axial component of velocity, and the integration on the RHS should cover all surfaces contributing to the change of momentum.

For a Newtonian fluid in an axially symmetric flow with no circumferential velocity components, the z-component of stress on each surface normal to the z-direction, pointing toward the inside of the control volume, is [14]

$$\begin{aligned} P_{zz} &= p - 2\mu\frac{\partial v_z}{\partial z} + \frac{2}{3}\mu\nabla\cdot\boldsymbol{v} \\ &= p - \frac{4}{3}\mu\frac{\partial v_z}{\partial z} + \frac{2}{3}\frac{\mu}{r}\frac{\partial}{\partial r}(rv_r), \end{aligned} \tag{3}$$

where the second viscosity coefficient has been taken approximately as $-\frac{2}{3}\mu$ and the following expression for veloc-

ity divergence $\nabla \cdot \boldsymbol{v}$ in cylindrical coordinates has been employed

$$\nabla \cdot \boldsymbol{v} = \frac{\partial}{\partial z}(v_z) + \frac{1}{r}\frac{\partial}{\partial r}(rv_r). \tag{4}$$

On each surface parallel to the z-direction, the z-component of the stress is [14]

$$P_{rz} = \mp\mu\left(\frac{\partial v_r}{\partial z} + \frac{\partial v_z}{\partial r}\right), \tag{5}$$

in which the minus applies to surfaces beneath the system, while the plus applies to surfaces above the system.

Applying Eqs. (2)–(5) to the control volume *D-E-N-M-F-G-H-I-J-D* shown in Fig. 3, we have

$$\begin{aligned}
&\int_D^E \left(p - \frac{4}{3}\mu\frac{\partial v_z}{\partial z}\right)2\pi r\mathrm{d}r - \int_E^N \mu\frac{\partial v_z}{\partial r}\cdot 2\pi r_E\mathrm{d}z \\
&\quad - \int_M^N \left(p - \frac{4}{3}\mu\frac{\partial v_z}{\partial z}\right)2\pi r\mathrm{d}r \\
&\quad + \int_F^G \left[p - \frac{4}{3}\mu\frac{\partial v_z}{\partial z} + \frac{2}{3}\frac{\mu}{r}\frac{\partial(rv_r)}{\partial r}\right]2\pi r\mathrm{d}r \\
&\quad + \int_G^H \mu\left(\frac{\partial v_r}{\partial z} + \frac{\partial v_z}{\partial r}\right)\cdot 2\pi r_H\mathrm{d}z \\
&\quad - \int_I^H \left(p - \frac{4}{3}\mu\frac{\partial v_z}{\partial z}\right)2\pi r\mathrm{d}r \\
&\quad + \int_J^D \left[p - \frac{4}{3}\mu\frac{\partial v_z}{\partial z} + \frac{2}{3}\frac{\mu}{r}\frac{\partial(rv_r)}{\partial r}\right]2\pi r\mathrm{d}r \\
&= -\int_F^G \rho v_z^2\cdot 2\pi r\mathrm{d}r + \int_G^H \rho v_r v_z\cdot 2\pi r_H\mathrm{d}z \\
&\quad - \int_J^D \rho v_z^2\cdot 2\pi r\mathrm{d}r,
\end{aligned} \tag{6}$$

where $D, E, \cdots, N$ denote the radii or axial positions at $D, E, \cdots, N$.

Noting that the sum of the 6th term on the LHS of Eq. (6) and $p_0 A_\mathrm{p}$ (Here p_0 and A_p are ambient pressure and plate surface area, respectively.) is the negative of the net force acting on the plate, i.e.,

$$F = \int_I^H \left[\left(p - \frac{4}{3}\mu\frac{\partial v_z}{\partial z}\right) - p_0\right]2\pi r\mathrm{d}r, \tag{7}$$

and if the three terms on the RHS of Eq. (6) are denoted as $-M_2$, M_3 and $-M_1$ as shown in Fig. 3, we obtain

$$\begin{aligned}
F = M_1 + M_2 - M_3 &+ \int_D^E \left(p - p_0 - \frac{4}{3}\mu\frac{\partial v_z}{\partial z}\right)2\pi r\mathrm{d}r \\
&- \int_E^N \mu\frac{\partial v_z}{\partial r}\cdot 2\pi r_E\mathrm{d}z \\
&- \int_M^N \left(p - p_0 - \frac{4}{3}\mu\frac{\partial v_z}{\partial z}\right)2\pi r\mathrm{d}r \\
&+ \int_F^G \left[p - p_0 - \frac{4}{3}\mu\frac{\partial v_z}{\partial z} + \frac{2}{3}\frac{\mu}{r}\frac{\partial(rv_r)}{\partial r}\right]2\pi r\mathrm{d}r \\
&+ \int_G^H \mu\left(\frac{\partial v_r}{\partial z} + \frac{\partial v_z}{\partial r}\right)2\pi r_H\mathrm{d}z \\
&+ \int_J^D \left[p - p_0 - \frac{4}{3}\mu\frac{\partial v_z}{\partial z} + \frac{2}{3}\frac{\mu}{r}\frac{\partial(rv_r)}{\partial r}\right]2\pi r\mathrm{d}r.
\end{aligned} \tag{8}$$

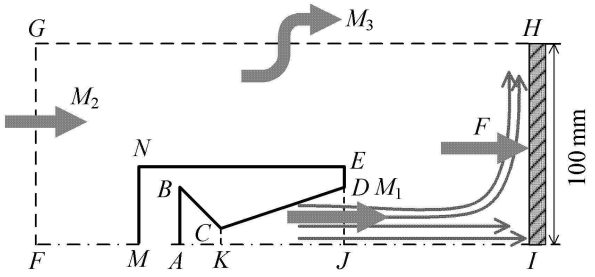

Fig. 3 Schematic diagram of relationship among z-momentums of a jet impinging on a flat plate

The first term M_1 on the RHS of Eq. (8) is the thrust force caused by the momentum flux of the gas jet exhausting from the nozzle, while the last term is the additional thrust force due to the difference between the normal stress at the nozzle exit section and the ambient pressure.

When and only when all the other terms except M_1 and the last term on the RHS are negligible, Eq. (8) is reduced to

$$\begin{aligned}
F &= M_1 + \int_J^D \left[p - p_0 - \frac{4}{3}\mu\frac{\partial v_z}{\partial z} + \frac{2}{3}\frac{\mu}{r}\frac{\partial(rv_r)}{\partial r}\right]2\pi r\mathrm{d}r \\
&= \int_J^D \rho v_z^2\cdot 2\pi r\mathrm{d}r + \int_J^D \left[p - p_0 - \frac{4}{3}\mu\frac{\partial v_z}{\partial z}\right. \\
&\quad \left. + \frac{2}{3}\frac{\mu}{r}\frac{\partial(rv_r)}{\partial r}\right]2\pi r\mathrm{d}r = T,
\end{aligned} \tag{9}$$

i.e., the force exerted on the plate by the impinging gas jet (F) is equal to the thrust force produced by the nozzle flow (T), and the thrust force T can be accurately measured by the impulse method ($F = T$).

Because those neglected terms are not really always negligible, F may be somewhat different from T. In the following, we will compare the thrust force T and the force F exerted on the plate by using a computational approach. It is noteworthy that Eqs. (3) and (5)–(9) are written for the laminar flow regime where only the molecular viscosity μ is involved. For the turbulent flow regime, the molecular viscosity μ appearing in those equations are substituted by $(\mu + \mu_\mathrm{t})$, where μ_t is the turbulent viscosity.

For the steady, turbulent and axially symmetrical flow, the following governing equations are employed in the computational study.

State equation

$$p = \rho RT, \tag{10}$$

Continuity

$$\frac{\partial}{\partial z}(\rho v_z) + \frac{1}{r}\frac{\partial}{\partial r}(r\rho v_r) = 0, \tag{11}$$

Axial and radial momentum

$$\frac{\partial(\rho v_z v_z)}{\partial z} + \frac{1}{r}\frac{\partial(r\rho v_z v_r)}{\partial r} = -\frac{\partial p}{\partial z} + 2\frac{\partial}{\partial z}\left[(\mu+\mu_t)\frac{\partial v_z}{\partial z}\right] + \frac{1}{r}\frac{\partial}{\partial r}\left[r(\mu+\mu_t)\left(\frac{\partial v_z}{\partial r}+\frac{\partial v_r}{\partial z}\right)\right] - \frac{2}{3}\frac{\partial}{\partial z}[(\mu+\mu_t)\nabla\cdot\boldsymbol{v}], \tag{12}$$

$$\frac{\partial(\rho v_z v_r)}{\partial z} + \frac{1}{r}\frac{\partial(r\rho v_r v_r)}{\partial r} = -\frac{\partial p}{\partial r} + \frac{2}{r}\frac{\partial}{\partial r}\left[r(\mu+\mu_t)\frac{\partial v_r}{\partial r}\right] + \frac{\partial}{\partial z}\left[(\mu+\mu_t)\left(\frac{\partial v_r}{\partial z}+\frac{\partial v_z}{\partial r}\right)\right] - 2(\mu+\mu_t)\frac{v_r}{r^2} - \frac{2}{3}\frac{\partial}{\partial r}[(\mu+\mu_t)\nabla\cdot\boldsymbol{v}], \tag{13}$$

Energy

$$\frac{\partial(\rho v_z h)}{\partial z} + \frac{1}{r}\frac{\partial(r\rho v_r h)}{\partial r} = \frac{1}{r}\frac{\partial}{\partial r}\left[r\left(\frac{k}{C_p}+\frac{\mu_t}{Pr_h}\right)\frac{\partial h}{\partial r}\right] + \frac{\partial}{\partial z}\left[\left(\frac{k}{C_p}+\frac{\mu_t}{Pr_h}\right)\frac{\partial h}{\partial z}\right] + v_z\frac{\partial p}{\partial z} + v_r\frac{\partial p}{\partial r} + \Phi, \tag{14}$$

Because compressible flow may be involved, the pressure work term $v_z\partial p/\partial z + v_r\partial p/\partial r$ and the viscous dissipation term Φ have been included in the energy equation (14). The expression for the viscous dissipation in $z-r$ cylindrical coordinates is

$$\Phi = (\mu+\mu_t)\left\{2\left[\left(\frac{\partial v_r}{\partial r}\right)^2 + \left(\frac{v_r}{r}\right)^2 + \left(\frac{\partial v_z}{\partial z}\right)^2\right] + \left(\frac{\partial v_r}{\partial z}+\frac{\partial v_z}{\partial r}\right)^2\right\} - \frac{2}{3}(\mu+\mu_t)(\nabla\cdot\boldsymbol{v})^2, \tag{15}$$

Turbulent kinetic energy

$$\frac{\partial(\rho v_z K)}{\partial z} + \frac{1}{r}\frac{\partial(r\rho v_r K)}{\partial r} = \frac{\partial}{\partial z}\left[\left(\mu+\frac{\mu_t}{Pr_K}\right)\frac{\partial K}{\partial z}\right] + \frac{1}{r}\frac{\partial}{\partial r}\left[r\left(\mu+\frac{\mu_t}{Pr_K}\right)\frac{\partial K}{\partial r}\right] + G - \rho\varepsilon, \tag{16}$$

Turbulent kinetic-energy dissipation rate

$$\frac{\partial(\rho v_z \varepsilon)}{\partial z} + \frac{1}{r}\frac{\partial(r\rho v_r \varepsilon)}{\partial r} = \frac{\partial}{\partial z}\left[\left(\mu+\frac{\mu_t}{Pr_\varepsilon}\right)\frac{\partial \varepsilon}{\partial z}\right] + \frac{1}{r}\frac{\partial}{\partial r}\left[r\left(\mu+\frac{\mu_t}{Pr_\varepsilon}\right)\frac{\partial \varepsilon}{\partial r}\right] + \frac{\varepsilon}{K}(C_1 G - C_2\rho\varepsilon), \tag{17}$$

The generation term G in Eqs. (16) and (17) is calculated by

$$G = \mu_t\left[2\left(\frac{\partial v_z}{\partial z}\right)^2 + 2\left(\frac{\partial v_r}{\partial r}\right)^2 + 2\left(\frac{v_r}{r}\right)^2 + \left(\frac{\partial v_z}{\partial r}+\frac{\partial v_r}{\partial z}\right)^2\right], \tag{18}$$

where μ_t is the turbulent viscosity and calculated by $\mu_t = c_\mu\rho K^2/\varepsilon$. C_μ, C_1, C_2, Pr_h, Pr_K and Pr_ε are constants in the K-ε two-equation turbulence model and are taken to be their commonly-used values, i.e., 0.09, 1.44, 1.92, 1.0, 1.0 and 1.3, respectively.

The domain *A-B-C-D-E-N-M-F-G-H-I-J-K-A* (Fig. 3) has been used in the computational study, containing the Laval nozzle and the flat plate impinged on by the gas jet. The throat radius of the nozzle $CK = 0.4$ mm, the width $MN = EJ = 4$ mm and the convergent and divergent semi-angles are 30° and 10°, respectively. The plate radius $HI = 100$ mm, and the distance between the nozzle exit and the plate is taken to be different values in the computation.

The boundary conditions used in the present study are as follows. At the inlet section of the nozzle, the mass flow rate is given and the gas temperature is taken to be 300 K. For turbulent equations, $K = 0.000\,05 \times v_z^2$ and $\varepsilon = (K^{3/2})/0.004\,175$ are given at the nozzle inlet. Non-slip conditions and wall-function treatment are employed at the solid wall; ambient pressure 1.013×10^5 Pa is adopted at free boundaries *F-G* and *G-H* for the atmospheric pressure cases and 23 Pa for low pressure cases. Along the axis of the computational domain, the axisymmetrical conditions are employed.

The numerical computation was carried out using the FLUENT code. The reliability of the computed results is checked by inspecting whether the mass flux conservation in the nozzle and Eq. (6) deduced from the momentum theorem are satisfied. In this computation, the residual errors of Eq. (6) are less than 6% and 1% for all atmospheric pressure cases and low pressure cases, respectively.

3 Results and discussion

3.1 Atmospheric pressure environment, cold flow

Figures 4–6 show the typical results of measurement of impinging force on the flat plate under various conditions. The nozzles used in the experiments are listed in Table 1.

Figure 4 shows that for each flow rate, there is a range of axial distance from the nozzle exit within which the measured force is constant, and this range is different for different gas flow rates, with the beginning point farther away for higher flow rates. In fact, for the highest flow rates in these tests, the plateau has not yet been reached. This plateau of measured force is considered corresponding to the situation where the presence of the plate has minimal influence on the nozzle flow, and best represents the nozzle thrust. When the

plate moves close to the nozzle exit, a sharp decrease in measured force occurs.

Table 1 Structures and dimensions of nozzles used in these studies

Nozzle	Divergent section half-angle/(°)	Divergent section length/mm	Throat diameters/mm
1	15	11	0.8
2	10	18	0.8
3	10	12	0.8
4	10	6	0.8
5	10	3.5	0.8

The measured plateau thrust becomes smaller when the nozzle is longer (larger expansion ratio). This phenomenon can be explained by the fact that in these tests, the high environmental pressure and the not-so-high supply pressures result in subsonic exit flow, with shock waves inside the divergent section of the nozzle, especially for the longer nozzles. Further expansion in the nozzle reduces the exit velocity, thus lowering the thrust. For short nozzles, the flow can be supersonic at the exit, and there would be no further deceleration inside the nozzle, causing less effect of the nozzle length on the thrust.

Figure 5 shows that the measured impinging force increases approximately linearly with increasing mass flow rate of the working gas for all the tested nozzles.

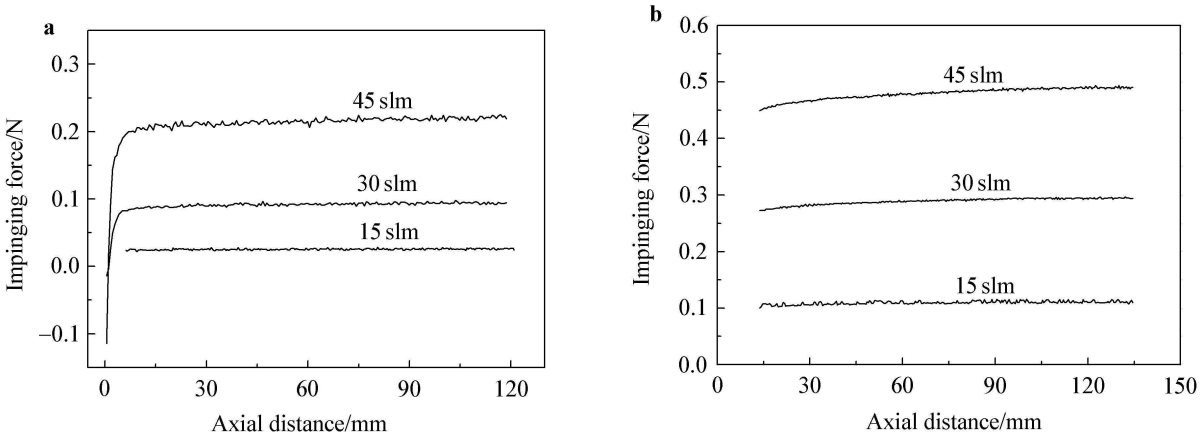

Fig. 4 Impinging force on the flat plate at various axial distances. Cold N_2, atmospheric environment. **a** Nozzle 2; **b** Nozzle 5

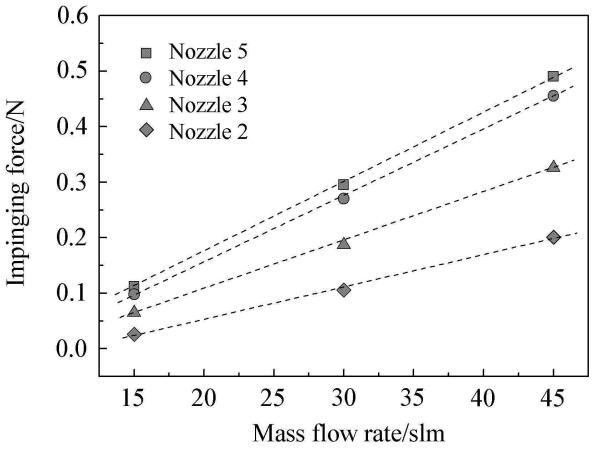

Fig. 5 Impinging force on flat plate at various gas flow rates. Cold N_2, atmospheric environment

Typical measurements of impact pressure distribution by (1) a pressure tap at the center of a flat plate swept across the jet cross section and (2) an impact pressure probe swept across the jet are shown in Fig. 6. The flow fields in these two cases are different: one corresponding to a stagnation flow of a jet against a flat plate, and the other corresponding to a disturbed free jet. Thus the measured values of pressure are also slightly different.

The first kind of measurement shows that for the jets tested, the size of the flat plate is large enough to fully capture the axial momentum of the jet, and the flow beyond a certain radius will not contribute to the axial force on the plate. The pitot probe measurements demonstrate typical flow field of a subsonic jet [15]. In an atmospheric pressure environment, with the flow rates and nozzle dimensions tested, the jet is either subsonic or quickly becomes subsonic after the nozzle exit. Therefore, the results actually describe the flow of subsonic jets impinging on a flat plate.

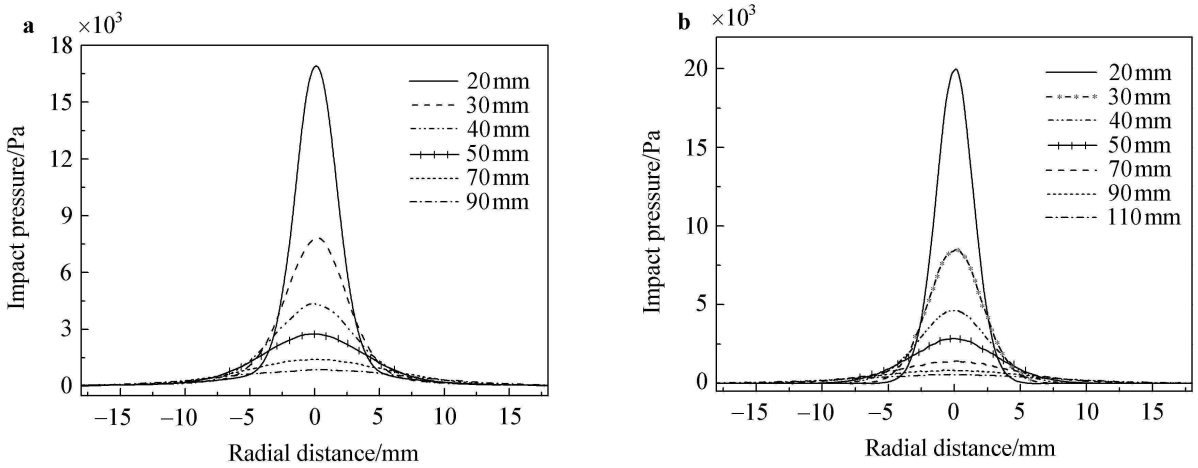

Fig. 6 Impact pressure profiles (Nozzle 5, cold N_2, atmospheric environment, flow rate 30 slm). **a** Pressure tap on flat plate; **b** Pitot pressure probe

Some computational results corresponding to these test conditions are shown in Fig. 7 for the case where the half-angle and length of the nozzle divergent section are 10° and 3.5 mm, respectively (corresponding to Nozzle 5 in the experiment).

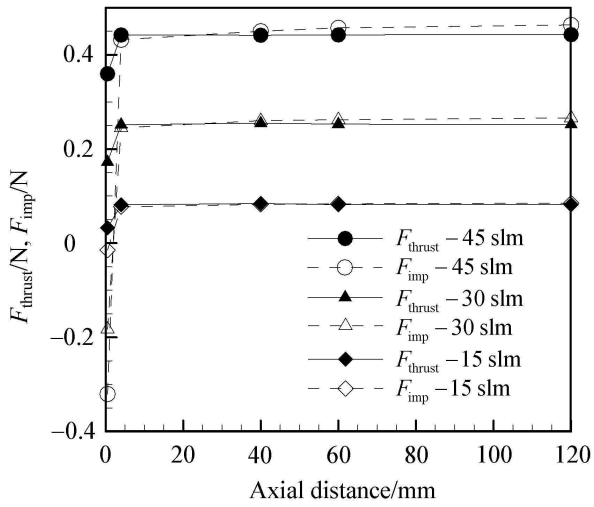

Fig. 7 Comparison of computed variation of nozzle thrust and impingement force of plate with the different plate standoff distance (atmospheric pressure)

In Fig. 7, F_{thrust} represents the computed thrust of the nozzle and F_{imp} represents the computed impingement force. It is shown that the computed thrust and impingement force are somewhat less than the corresponding measured results of impingement force with the same mass flow rates. Exact comparison of values of thrust between the experimental and computational results is not attempted because of the relatively arbitrary choice of some parameters used in the computational code and the resulting quantitative inaccuracy when used in such a complicated flow field, and unavoidable experimental inaccuracies. However, the general picture of the flow field and trends of variation compared with experiments provide insights into the mechanism of impingement force of the jet on the flat plate and the range of applicability of using the impulse method for thrust measurement. Figure 7 shows that there is a range of axial distance from the nozzle exit within which the computed impingement force is constant. This variation trend is similar to that of experimental cases mentioned above. It is also shown in Fig. 7 that the computed impingement forces are slightly different from the nozzle thrust, especially for the case with a higher flow rate. It is believed that this difference is either an indication of the deviation of the actual flow from the ideal conditions which results in the equality of the two quantities, or caused by the inappropriate boundary condition and other errors of numerical modeling.

As mentioned above, it is not the purpose in this work to make accurate comparison between the numerical computational results and the experimental data. Yet, comparing the data in Fig. 7 and Fig. 4b, which both correspond to the conditions of Nozzle 5, we found that the trend of a force plateau is evident in both cases, and the values of the measured and computed forces differ by only about 10%. This can be considered as a good qualitative agreement in the present situation.

Figure 8 presents the computed Mach number distributions within and outside the nozzle. It is shown that the pressure at the nozzle exit is lower than the atmospheric pressure and hence the nozzle jet flow is in over-expanded state. The computed data demonstrate that large fluctuations of Mach number exist at the downstream section of the expansion part of the nozzle. Due to the viscous dissipation, the fluctuation magnitudes of the jet parameters reduce rapidly in the flow direction, and the nozzle jet changes its flow regime from supersonic to subsonic flow.

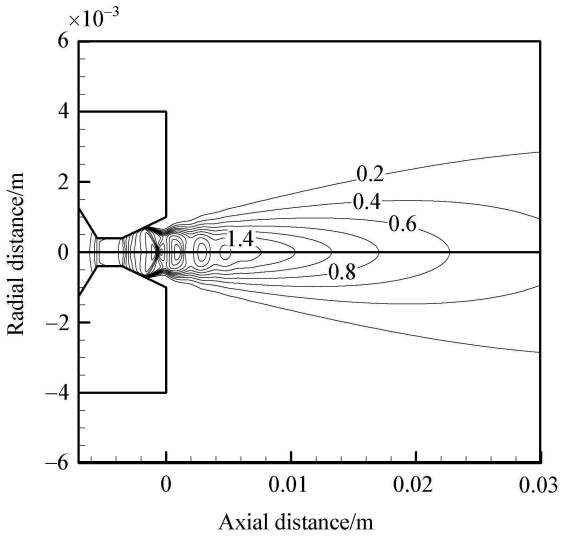

Fig. 8 Computed Mach number distributions in the turbulent nozzle jet for the case with the mass flow rates 45 slm. The Mach contour intervals are 0.2. The plate standoff distance is 120 mm

Figures 9 show the computed streamlines for the cases that plate standoff distances are 4 mm and 120 mm, respectively. The computational results show a region of strong influence when the plate is near the nozzle exit, and less influence as the plate is moved further away. These results agree with the experimental trends. When the flow rate is small, influence of the plate becomes less, as can be inferred from the flow fields shown in Fig. 9 and agreeing with the force measurement results shown in Fig. 4.

In these experiments, with the given supply pressure and the expansion ratio of the nozzles, the jet is either subsonic at the exit or quickly becomes subsonic at a short distance beyond the exit, as seen from the computed flow fields. Thus the influence of the flat plate would be felt throughout the region between the nozzle and the plate. When the plate is far enough from the nozzle, yet not too far from it such that the plate is still large enough to capture all the momentum of the jet, the conditions for $T = F$ would be better satisfied, and the measured force would be independent of the distance where the plate is placed. When the plate is moved too close to the nozzle (at a distance dependent not only on the nozzle diameter but also on the flow rate), the flow in the nozzle would be affected. The exit velocity would decrease, and so would the momentum and thrust. With varying lengths of the nozzle, the exit velocity decreases with the longer nozzles (subsonic flow, larger exit area), resulting in the decrease in thrust as shown in Fig. 5.

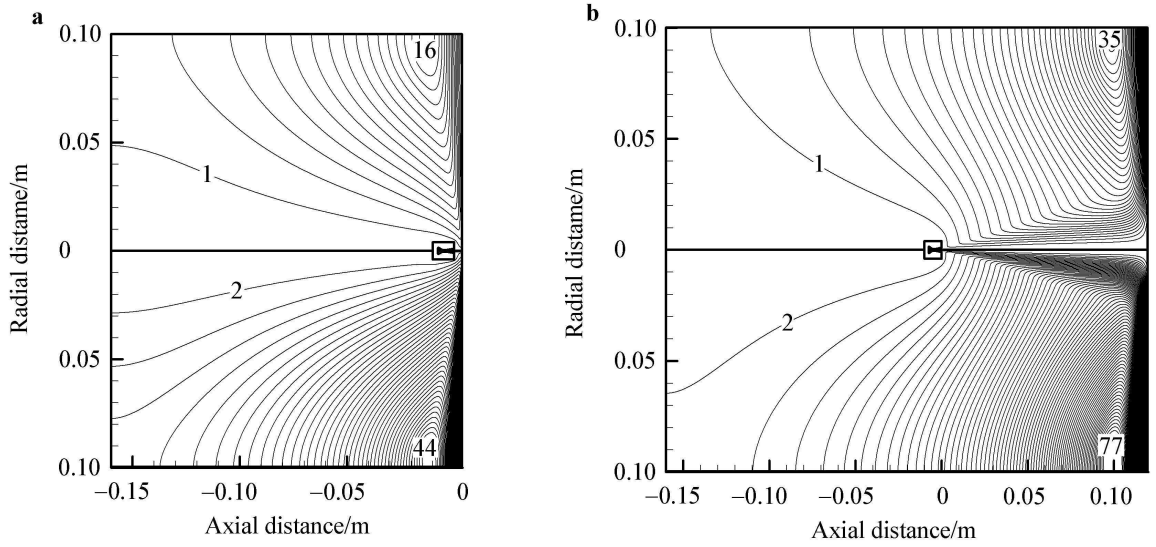

Fig. 9 Comparison of the computed streamlines in the turbulent nozzle jet for the case with the mass flow rates 15 slm in (upper semi-planes) and 45 slm in (lower semi-planes). Streamline intervals are 6.28×10^{-4} kg/s. **a** The plate standoff distance is 4 mm; **b** The plate standoff distance is 120 mm

3.2 Low pressure environment

With the vacuum system in operation, the environment pressure could be kept to the order of 20–70 Pa, depending on the gas flow rate. Figures 10–11 show the impinging force on the plate measured under various conditions.

As shown in Fig. 10, plateaus of measured force exist, which indicates that the conditions for the measurement principle are better satisfied. However, the plateaus are not exactly flat, especially at higher flow rates. This may have been caused by the variation in the impacted flow field which is complicated by the shock and rarefaction waves in the free jet, and the condition of zero z-momentum exiting in the control volume is not exactly satisfied. Or, when the vacuum

pumps were running, there were some interference caused by the vibrations, and the readings were not as steady as when there was no pumping. This situation needs to be further explored or improved in the future. Figure 11 demonstrates that the measured impinging force also increases approximately linearly with increasing gas flow rate for this low pressure case.

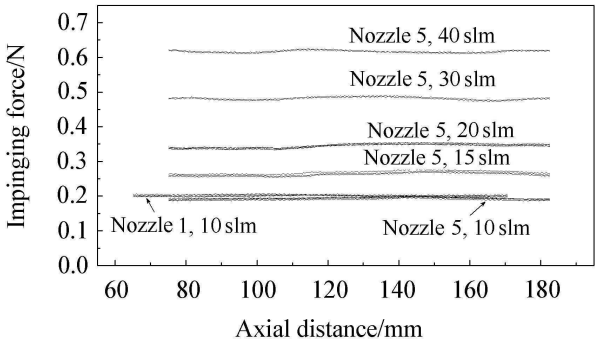

Fig. 10 Impinging force at varying distances from the nozzle exit (cold N_2, low pressure environment) (Nozzle 1: flow rate of 10 slm, Environment pressure 21.9 Pa; Nozzle 5: 10 slm, 22.5 Pa; 15 slm, 29.7 Pa; 20 slm, 37.4 Pa; 30 slm, 51.8 Pa; 40 slm, 66.9 Pa)

Pressure measurements with the pressure tap on the flat plate and the impact pressure probe are shown in Fig. 12.

The pressure distributions show the typical continuum underexpanded supersonic jet flow with expansion and shock wave reflections. The plateau of measured force at various distances under these conditions of the jet demonstrates the applicability of the basic principle in all cases.

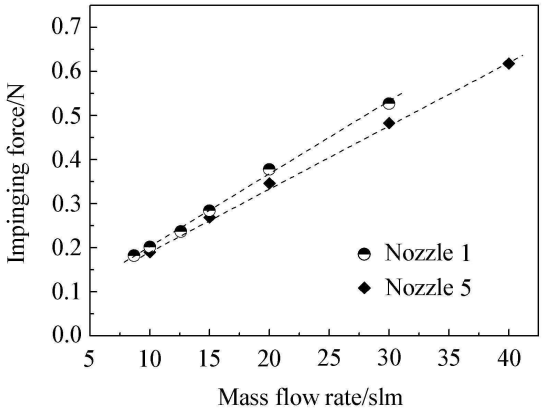

Fig. 11 Impinging force on flat plate at various gas flow rates (cold N_2, low pressure environment) (Nozzle 1: 8.7 slm, 19.6 Pa; 10 slm, 21.9 Pa; 12.6 slm, 25.2 Pa; 15 slm, 29.3 Pa; 20 slm, 36.4 Pa; 30 slm, 51.4 Pa; Nozzle 5: 10 slm, 22.5 Pa; 15 slm, 29.7 Pa; 20 slm, 37.4 Pa; 30 slm, 51.8 Pa; 40 slm, 66.9 Pa)

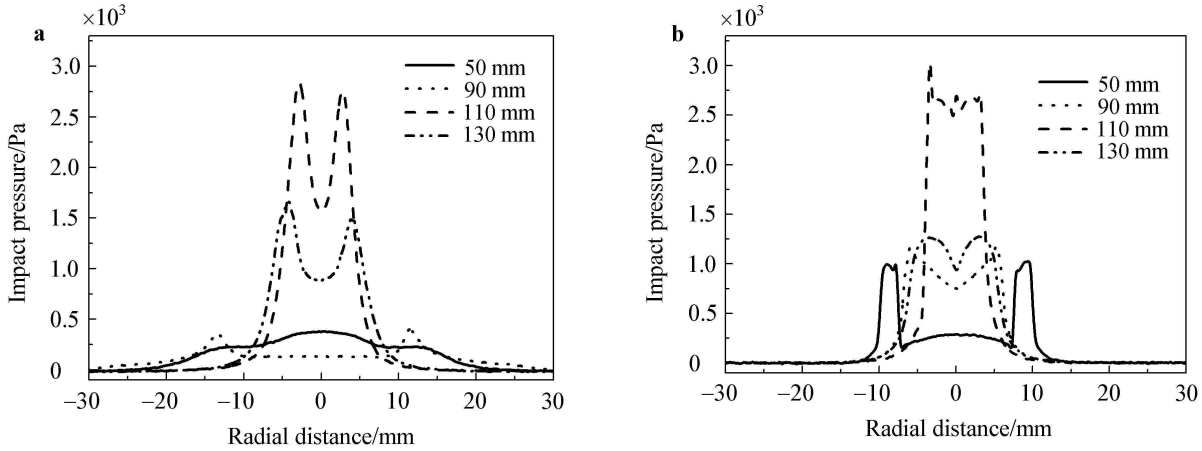

Fig. 12 Radial distribution of impact pressure (cold N_2, Low pressure environment, 21.9 Pa), Nozzle 1, flow rate 10 slm. **a** Pressure tap on flat plate; **b** Pitot pressure probe

Computed results for the low environment pressure case are shown in Figs. 13 and 14. For the low environment pressure cases, the pressure is set to be 23 Pa in our modeling. Figure 13 shows the computed variation of nozzle thrust and impingement force on the plate with different plate standoff distances. These computed data demonstrate that there exists a plateau for nozzle thrust and impingement force. These results agree with the experimental trends. Again, the computed value of force agrees with the experimental one, being within 10% (see Fig. 10).

With low environmental pressure, the pressure at the nozzle exit is higher than the environment pressure and hence

the nozzle jet is in the under-expanded state as shown in Fig. 14. The jet will continue to expand until the jet pressure becomes lower than the environment pressure. The expansion and compression waves will appear in the jet and they adjust the jet pressure to finally match itself with the environment pressure. Figure 14 shows that the jet keeps its flow regime of the supersonic flow within a longer distance after exhausting from the nozzle than that of atmospheric pressure cases. Figure 14a also shows that the entrainment rate of the nozzle jet in low pressure environment is much smaller than that of cases in atmospheric pressure.

The computed pressure distributions on the plate surface in low pressure environment also show some characteristics different from the atmospheric pressure cases, indicating the existence of shock and expansion waves in the flow field of the plume. However, direct comparison of the experimental and computed pressure distributions is not attempted because of the complexity of the flow field, which is difficult to describe in detail by the present computation method.

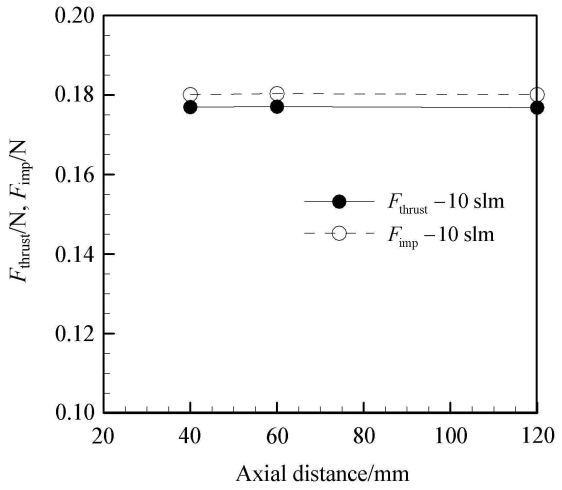

Fig. 13 Comparison of computed variation of nozzle thrust and impingement force of plate with the different plate standoff distance (low pressure)

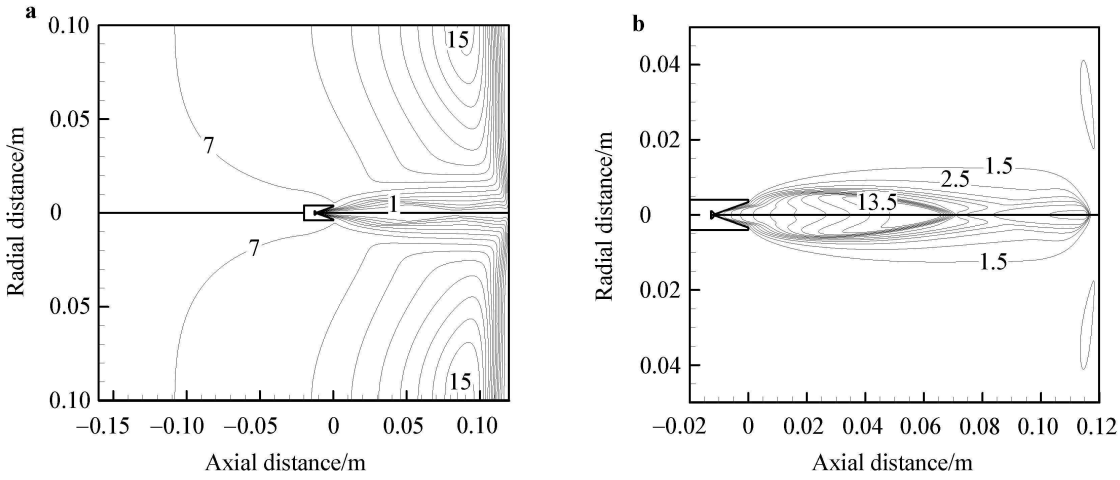

Fig. 14 Computed streamlines **a** and Mach number **b** distributions in the turbulent nozzle jet for the case with the mass flow rates 10 slm. The plate standoff distance is 120 mm. Streamline intervals are 3.14×10^{-5} kg/s in **a** and Mach contour intervals are 1.0 in **b**

3.3 Arc-heated jet

The force and impact pressure measurements for an arc-heated N_2/H_2 jet operated in low-pressure environment are shown in Fig. 15. The environmental pressure was kept at 10 Pa. A plateau of measured impact force at varying distances from the nozzle exit is observed. The impact pressure measurements show profiles different from the cold gas flow field at low environmental pressure. No clear wave structures were observed. This could be caused by the high temperature of the gas with the corresponding low density, exhibiting the effect of gas rarefaction.

Some photographs of arc-heated argon jets impinging on a flat plate are shown in Fig. 16. These pictures do not show the wave structures in the flow field of typical under-expanded supersonic jets in cold flows. The explanation could be sought in the rarefied nature of the flow under these extremely high temperature conditions and needs further study. However, these photos, being able to qualitatively show the temperature distribution by the brightness, demonstrate a region indicative of a normal shock near the flat plate, high temperature regions near the plate and in the flow away from the center of the plate. These observations agree qualitatively with numerical computations.

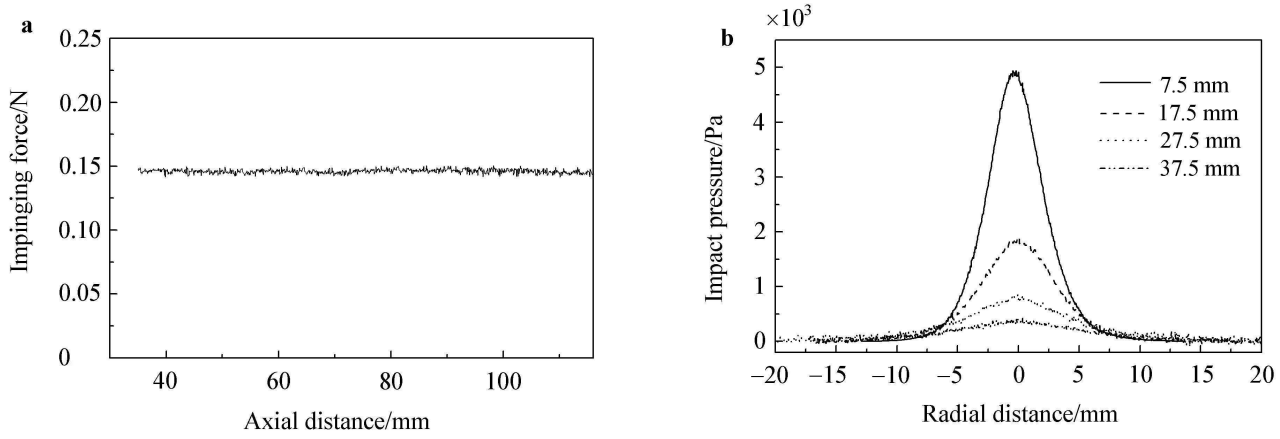

Fig. 15 Arc-heated N_2/H_2 jet in low-pressure environment (N_2/H_2 volume ratio 1:2, total flow rate 4.5 slm, arc current 7.5 A, voltage 120 V). **a** Impinging force at various distances; **b** Pitot pressure radial distribution

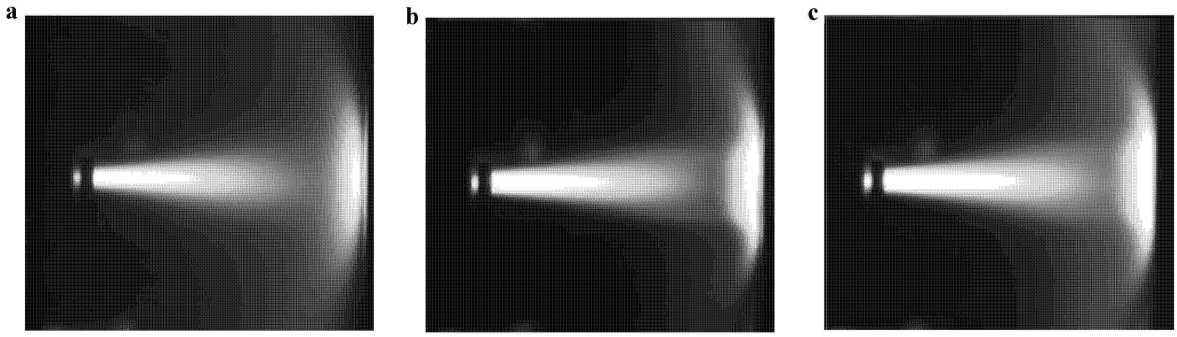

Fig. 16 Photographs of arc-heated argon jets impinging on a flat plate. **a** 3.4 slm, 8 A; **b** 9 slm, 8 A; **c** 9 slm, 12 A

Some discussion on the effects of gas rarefaction is in order here. The rarefied gas effects show up when the *Kn* number, defined by the ratio of gas particle mean free path to the relevant local geometrical dimension, becomes large. In the cases of the present study, we need to look at the range of *Kn* numbers to see when it is necessary to take the rarefied gas effects into consideration.

The gas particle mean free paths for the cases in this study have been estimated from the parameters of the flow fields. For a cold subsonic jet under atmospheric environment, λ (mean free path) is of the order of 0.1 μm, definitely a continuum for all cases considered. The cold supersonic jets at low pressures in the range of the present study had λ of the order of 0.3 mm in the free stream when the pressure reaches the low value of the ambient. However, at the pressure levels at the nozzle exit and on the surface of the flat plate where the jet impinges, λ is very much smaller. Thus the continuum assumption and no-slip boundary condition are still valid in the computations. The arc-heated jets at low pressure had λ of the order of several mm in the free stream. This is large compared with the diameter of the measured hole of the pressure probe or the thickness of ordinary shock waves, so the flow would exhibit characteristics of a rarefied gas for these cases. However, because the flat plate for measuring the impinging force is very large compared with λ of the compressed gas near the plate in the present case, the effect on the indirect method of thrust measurement is still small. Only when the environmental pressure is very low (near vacuum as in some test facilities, e.g., for testing ion engines or Hall thrusters) where λ could be very large, the possible reflections of gas particles from the surface of the flat plate are considered or avoided for the measurement, because they will possibly cause deviations from the requirement of zero axial momentum flux out of the control volume. The exact amount of error that might be introduced under such conditions would depend on the degree of rarefaction, the surface condition and/or the shape of the impinged plate, and needs to be studied further by both experimental and numerical methods.

The above discussion indicates that the impulse method of indirect thrust measurement, when properly applied, is valid in all these conditions. However, care must be exercised to know the range of applicability and limits of its accuracy, and to avoid possible sources of error.

The above results give a general picture of the flow of a jet impinging normally on a flat plate at various distances and the force acting on it, which could have direct implications for the method of indirect thrust measurement. The studies show that certain requirements have to be satisfied in the flow field before the method can be comfortably used to measure the thrust, and careful work would be involved in each case to ensure the proper requirements are met. However, because the fulfillment of the conditions for equality of the impinging force and the jet thrust is manifested in a measured force plateau with distance, this could be a simple guideline in practice for the proper use of the impulse method, i.e., when using the impulse method with the flat plate for indirect thrust measurement, the distance between the plate and the jet exit should be varied, and the readings should be taken within the range of the plateau of force. Actually, experiments reported previously are usually conducted within this range, but the test results would be doubly reassuring if such a check is carried out.

4 Conclusions

Aerodynamic aspects of the jet impinging on a flat plate in relation to the indirect thrust measurement have been studied both experimentally and numerically. We concluded as follows:

The impulse method is a reliable method for indirect thrust measurement if the following criteria are satisfied:

(1) No axial momentum carried out around the edge of the flat plate—large enough plate at not too great a distance
(2) No reflection of the jet or particles at the surface of the flat plate—proper aerodynamics or special construction of the impulse receiver. If the environmental pressure is extremely low, the reflection of particles should be avoided.
(3) No influence on the nozzle flow by the presence of the flat plate—the plate not too close to the nozzle exit, especially for high environmental pressure or high flow rates.

Usually for ordinary test facilities, satisfactory measurement can be ensured within the range where the measured impinging force does not change with distance from the nozzle exit. This can be a simple guideline for the proper use of the impulse method for indirect thrust measurement.

Acknowledgement Very helpful discussion with Prof. D. Y. Liu is gratefully acknowledged.

References

1 Böhrk, H., Auweter-Kurtz, M.: Thrust measurement of the hybrid electric thruster TIHTUS by a baffle plate. J. Propulsion and Power **25**(3), 729–736 (2009)
2 Longmier, B.W., Reid, B.M., Gallimore A.D., et al.: Validating a plasma momentum flux sensor to an inverted pendulum thrust stand. J. Propulsion and Power **25**(3), 746–752 (2009)
3 West, M.D., Charles, C., Boswell, R.W.: A high sensitivity momentum flux measuring instrument for plasma thruster exhausts and diffusive plasmas. Rev. Sci. Instrum. **80**, 053509 (2009)
4 Cen, J.W., Xu, J.L.: Experimental investigation on the relation between micro-thrust and impinging force. J. Propulsion Technology **30**(1), 114–118 (2003) (in Chinese)
5 Takao, Y., Eriguchi, K., Ono, K.: A miniature electrothermal thruster using microwave-excited microplasmas: thrust measurement and its comparison with numerical analysis. J. App. Phys. **10**(1), 123307 (2007)
6 Chavers, D.G., Chang-Díaz, F.R., Irvine, C., et al.: Momentum and heat flux measurements using an impact target in flowing plasma. J. Propulsion and Power **22**(3), 637–644 (2006)
7 Paxson, D.E., Wilson, J., Dougherty, K.T.: Unsteady ejector performance: an experimental investigation using a pulsejet driver. AIAA Paper 2002-3915 (2002)
8 Hiers, R., Pruitt, D.: Determination of thrust from pitot pressure measurements. AIAA Paper 2001-3314 (2001)
9 Tang, F., Ye, X.Y., Zhou, Z.Y.: A target indirect measurement method of microthrust. Micronanoelectronic Technology **40**(7-8), 438–440 (2003) (in Chinese)
10 Gessini, P., Gabriel, S.B.: Hollow cathode thrust measurement using a target: system development and calibration. AIAA Paper 2002-4104 (2002)
11 Mizukaki, T.: Visualization and force measurement of high-temperature, supersonic impulse jet impinging on baffle plate. J. Visualization **10**(2), 227–235 (2007)
12 Shapiro, A.H.: The Dynamics and Thermodynamics of Compressible Fluid Flow. Wiley, New York, 16–19 (1953)
13 White, F.M.: Fluid Mechanics. McGraw-Hill, New York, 144 (1959)
14 Hughes, W.F., Gaylord, E.W.: Basic Equations of Engineering Science. McGraw-Hill, New York, 1–15 (1964)
15 Abramovich, G.N.: The Theory of Turbulent Jets. MIT Press, Cambridge, (1963)